High-pressure alloying of iron and xenon: "Missing" Xe in the Earth's core?

Kanani K. M. Lee[1,2,3] and Gerd Steinle-Neumann[2]

[1] Ab initio quantum mechanical calculations show that xenon (Xe) can be alloyed with hexagonal close-packed iron at high pressure through substitutional incorporation, with a favorable enthalpy of formation for the alloy relative to the separate elemental solids, suggesting that Xe is soluble in the Earth's iron-rich core (up to ∼0.8 mol %). This alloying behavior and the possible presence of a significant amount of Xe in the core are important for understanding the accretion and evolution of the Earth and its atmosphere.

Citation: Lee, K. K. M., and G. Steinle-Neumann (2006), High-pressure alloying of iron and xenon: "Missing" Xe in the Earth's core?, *J. Geophys. Res.*, *111*, B02202, doi:10.1029/2005JB003781.

1. Introduction

[2] With its inherent chemical inertness, noble gas xenon has been used to study the evolution of Earth and its atmosphere through investigation of the daughter products from short-lived radioactive isotopes (e.g., $^{129}I \rightarrow {}^{129}Xe$ and ^{244}Pu (or ^{238}U) $\rightarrow {}^{136}Xe$ systematics) [*Farley and Neroda*, 1998; *Ozima and Podosek*, 1999]. However, the Earth is "missing" Xe in its atmosphere: Xe is depleted compared with chondritic abundances and lighter noble gases [*Krummenacher et al.*, 1962; *Pepin*, 1991]. It has been concluded that more than 90% of the Earth's Xe budget is missing; however, the loss mechanism is less obvious. Many models have attempted to explain Earth's Xe depletion [*Dauphas*, 2003; *Pepin*, 1991; *Pepin and Porcelli*, 2002; *Porcelli and Ballentine*, 2002; *Tolstikhin and O'Nions*, 1994]. Mere hydrodynamic escape or impact vaporization is not enough to account for the missing Xe since even lighter rare gases like argon and neon are less depleted than heavier xenon. Additionally, extensive searches for surface Xe reservoirs were conducted to find the missing xenon since Xe is more readily adsorbed into ice [*Bernatowicz et al.*, 1985; *Wacker and Anders*, 1984] and sediments [*Bernatowicz et al.*, 1984; *Matsuda and Matsubara*, 1989] than lighter rare gases. None of these studies found such a Xe reservoir. Instead, the missing Xe may be hidden deep in the Earth's interior where there is little communication with the surface [*Jephcoat*, 1998].

[3] Here we consider the likelihood of xenon in the Earth's core through the formation of a high-pressure alloy with iron. In light of recent experimental [*Balog et al.*, 2003; *Lee and Jeanloz*, 2003; *Lin et al.*, 2002] and theoretical [*Alfe et al.*, 2000a; *Lee et al.*, 2004] results on high-pressure alloying of iron with various elements (e.g., sulfur, silicon, and potassium), the pressure-induced insulator-metal transition in Xe at pressures above ∼125 GPa [*Eremets et al.*, 2000; *Goettel et al.*, 1989; *Reichlin et al.*, 1989] and the close-packed nature of Fe and Xe at high pressure extends the possibility of Xe forming a solid solution with the high-pressure form of iron, hexagonal close-packed (hcp) ε-Fe, thought to be stable in the Earth's inner core. While ε-Fe is only expected to be stable and present in the solid inner core, liquid iron, present in the outer core, has been found to be close packed with a coordination number similar to that of solid ε-Fe [*Alfe et al.*, 2000b]; therefore, in this study we focus on ε-Fe and assume the solubility of Xe into the crystalline structure will be near that of the liquid.

2. Methods

[4] The electronic structure and energetics of the Fe-Xe supercells, as well as those of the elemental end-members Fe and Xe, have been calculated by density functional theory (DFT)-based electronic structure methods. DFT is exact except for the basic approximation for exchange and correlation that describes the many-body interactions of electrons in the system. Most recent computational work on the noble gases, in particular Xe [*Caldwell et al.*, 1997; *Cohen et al.*, 1997; *Dewhurst et al.*, 2002; *Tsuchiya and Kawamura*, 2002], has used the local density approximation, whereas properties of transition metals, like iron, are more successfully described with the generalized gradient approximation (GGA) [*Perdew et al.*, 1992]. Because of its success with Fe and as we study compositions close to pure Fe we chose to use the GGA for Fe, Xe, and the Fe-Xe compounds in order to assure compatibility of results (see auxiliary material[1]). We use the projector augmented wave method (PAW) [*Kresse and Joubert*, 1999] as implemented in the Vienna Ab initio Simulation Package [*Kresse and Furthmuller*, 1996; *Kresse and Hafner*, 1993]. As we consider high compressions resulting in hybridization of

---

[1]Division of Geological and Planetary Sciences, California Institute of Technology, Pasadena, California, USA.
[2]Bayerisches Geoinstitut, Universität Bayreuth, Bayreuth, Germany.
[3]Now at Physics Department, New Mexico State University, Las Cruces, New Mexico, USA.

Table 1. Vinet Equation of State Parameters for Fe and Fe-Xe Alloys[a]

	Supercell Size	V_0, Å^3	K_0, GPa	K_0'	E_0, eV	c/a Range	Xe Concentration, wt % ppm
$Fe_{0.9688}Xe_{0.0312}$	32	10.69	253	5.08	−7.7899	1.592−1.597	∼70,000
$Fe_{0.9792}Xe_{0.0208}$	48	10.54	263	5.01	−7.9855	1.592−1.602	∼48,000
$Fe_{0.9896}Xe_{0.0104}$	96	10.39	275	4.93	−8.1760	1.596−1.603	∼24,000
$Fe_{0.9931}Xe_{0.0069}$	144	10.34	278	4.91	−8.2404	1.581−1.597	∼16,000
$Fe_{0.9944}Xe_{0.0056}$	180	10.32	282	4.87	−8.2708	1.586−1.599	∼13,000
$Fe_{0.9958}Xe_{0.0042}$	240	10.30	282	4.88	−8.2951	1.583−1.598	∼9,700
Fe	−	10.25	286	4.85	−8.3676	1.6	−

[a]See *Vinet et al.* [1989]. Room pressure volume, V_0; bulk modulus, K_0; its pressure derivative, K_0'; and energy, E_0.

low-lying electronic states in both Fe and Xe [*Cohen et al.*, 1997], we chose potentials that treat the $3p$, $3d$ and $4s$ states of iron and the $5s$ and $5p$ states for xenon as valence electrons.

[5] To compare the energetics of alloying and to test the PAW potentials used, we perform computations on iron in the hcp phase and on xenon in the face-centered cubic (fcc) and hcp structures. For the plane wave computations the critical computational parameters are the cutoff energy for the expansion of the charge density in a plane wave basis (E_{cut}) and the number of reciprocal space vectors at which the Kohn–Sham equations are solved (k points). The hcp cells of iron and xenon are based on an orthorhombic description of the hcp cell (space group *Pmma* with four atoms per cell, atoms at Wyckoff positions $2f$ and $2e$ with $z = 1/3$ and $1/6$, respectively) with cell edges of relative lengths of $\sqrt{3}$, 1, and the value of the c/a ratio, a k point mesh of $6 \times 8 \times 6$ and $E_{cut} = 300$ eV. We set the free parameter in the unit cell, the axial ratio c/a, to 1.6 for Fe and set the ideal close-packing value $\sqrt{(8/3)}$ for Xe. In both cases this is close to the experimentally and computationally determined axial ratio [*Cohen et al.*, 1997; *Jephcoat et al.*, 1987; *Mao et al.*, 1990; *Ross and McMahan*, 1980; *Steinle-Neumann et al.*, 1999]. For Xe we find only small changes in the energetics in response to relaxing the c/a ratio, justifying the choice of ideal c/a here and in previous computational studies [*Cohen et al.*, 1997; *Dewhurst et al.*, 2002]. For Xe we perform computations on the low-temperature, ambient pressure Xe I structure (fcc) and the high-pressure phase Xe II (hcp). We find, like others, that the fcc and hcp structures of Xe are closely related, showing little difference in energetics and equations of state [*Caldwell et al.*, 1997; *Dewhurst et al.*, 2002; *Tsuchiya and Kawamura*, 2002]. Although the equations of state are similar, we chose to use the high-pressure hcp structure of Xe in our comparisons of the Gibbs free energies of the pure elements with that of the Fe-Xe alloys (see Table S1 in auxiliary material). We also obtain good agreement for our Fe calculations with previous studies [*Steinle-Neumann et al.*, 1999] (see Table S1 in auxiliary material).

[6] The Fe-Xe supercells are based on the same orthorhombic description of the hcp cell as used for the pure element calculations. The supercells consist of $2 \times 2 \times 2$ (32 atoms), $2 \times 3 \times 2$ (48 atoms), $2 \times 4 \times 3$ (96 atoms), $3 \times 4 \times 3$ (144 atoms), $3 \times 5 \times 3$ (180 atoms), and $3 \times 5 \times 4$ (240 atoms) orthorhombic cells. Forces on the atoms occur in response to the incorporation of xenon. The atoms are relaxed self-consistently into their instantaneous ground state position with a quasi-Newtonian algorithm. To alleviate any nonhydrostatic stress on the lattice that is induced by

the large Xe atom, we relax the initial axial ratio in the hcp cell chosen to be that of iron ($c/a = 1.6$). Nonhydrostatic stresses were small, resulting only in a slight modification to c/a (Table 1).

[7] As we establish the energetics of formation of the Fe-Xe compounds, we must assure that absolute energies are well converged with respect to computational parameters. We have performed convergence tests for the 32-atom Fe-Xe supercell and the hcp phases of Fe and Xe. With a k point mesh of $3 \times 4 \times 3$ for the 32-atom supercell and $E_{cut} = 300$ eV, energy differences between the supercells and the elemental solids are converged to within 5 meV/atom. For the larger cells we chose nearly equivalent k point meshes of $3 \times 3 \times 3$, $3 \times 2 \times 2$, $2 \times 2 \times 2$, $2 \times 2 \times 2$, and $2 \times 2 \times 2$ for 48, 96, 144, 180, and 240 atoms, respectively.

[8] There are two incorporation mechanisms of elements into a metallic hcp structure: substitution and two possibilities of interstitial occupation, tetrahedral or octahedral incorporation [*Hume-Rothery*, 1963]. We use the supercells to study substitution and interstitial behavior. For each mechanism, one xenon atom is substituted on an hcp lattice site with 32, 48, 96, 144, 180, and 240 Fe atoms (essentially $Fe_{0.9688}Xe_{0.0312}$, $Fe_{0.9792}Xe_{0.0208}$, $Fe_{0.9896}Xe_{0.0104}$, $Fe_{0.9931}Xe_{0.0069}$, $Fe_{0.9944}Xe_{0.0056}$, and $Fe_{0.9958}Xe_{0.0042}$) over a wide compression range and incorporated interstitially on the tetrahedral and octahedral sites at two volumes, corresponding to ambient pressure and a compression of $V/V_0 = \sim 0.7$. We find that for Fe-Xe alloys the substitution mechanism of forming a solid solution is energetically more favorable than interstitial octahedral or tetrahedral incorporation at all concentrations and compressions tested; hence we focus on the substitutional incorporation mechanism. This result is similar to the behavior of iron-potassium alloys where a much larger atom is placed in the confines of a small, closely packed structure [*Lee et al.*, 2004].

[9] We have performed computations over a wide compression range from overexpanded to highly compressed volumes. The energy-volume relations for Fe, Xe, and Fe-Xe supercells are fit with a Vinet equation of state [*Vinet et al.*, 1989] as this expression is suitable for very compressible materials such as Xe [*Cohen et al.*, 2000] while also fitting both Fe and Fe-Xe supercells well (i.e., comparable to third-order finite strain expressions [*Birch*, 1952]) (Table 1, see also auxiliary material).

3. Results

[10] We compare the Gibbs free energy difference at static conditions (i.e., enthalpy) for the equilibrium
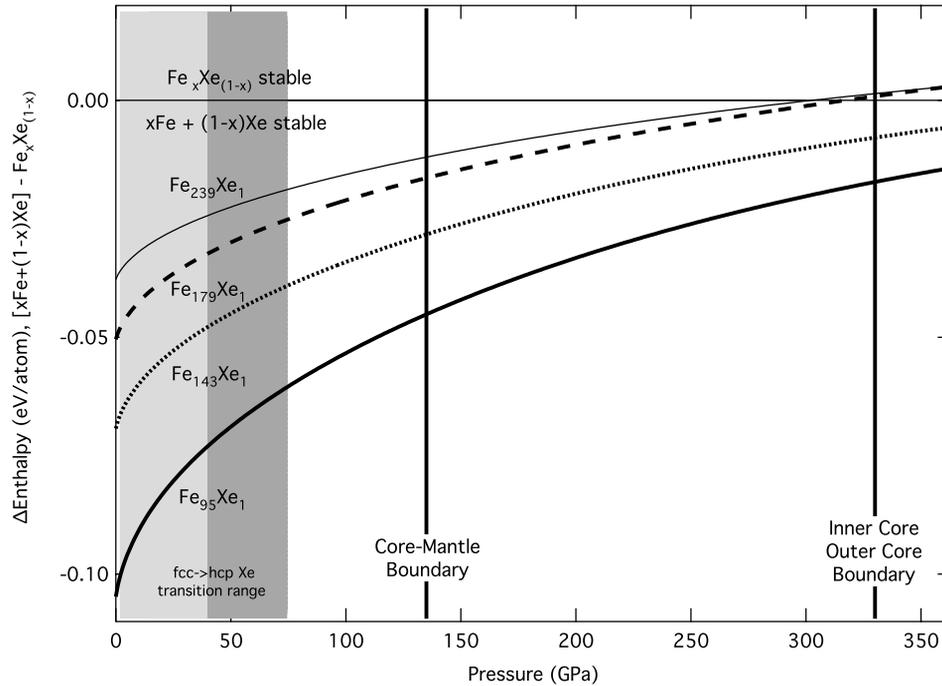
Figure 1. Difference in the enthalpy of the pure elements Fe and Xe compared with the Fe-Xe alloy versus pressure: $x\mathrm{Fe} + (1 - x)\mathrm{Xe} \iff \mathrm{Fe}_x\mathrm{Xe}_{(1-x)}$, where x is a value between 0.9896 and 0.9958 (96- to 240-atom supercells). Curves are labeled for the different Xe concentrations: $\mathrm{Fe}_{0.9958}\mathrm{Xe}_{0.0042}$ ($\mathrm{Fe}_{239}\mathrm{Xe}_1$, ~9700 ppm, thin); $\mathrm{Fe}_{0.9944}\mathrm{Xe}_{0.0056}$ ($\mathrm{Fe}_{179}\mathrm{Xe}_1$, ~13,000 ppm, dashed); $\mathrm{Fe}_{0.9931}\mathrm{Xe}_{0.0069}$ ($\mathrm{Fe}_{143}\mathrm{Xe}_1$, ~16,000 ppm, dotted); and $\mathrm{Fe}_{0.9896}\mathrm{Xe}_{0.0104}$ ($\mathrm{Fe}_{95}\mathrm{Xe}_1$, ~24,000 ppm, thick). For positive values the $\mathrm{Fe}_x\mathrm{Xe}_{(1-x)}$ alloy is energetically favored over the pure elements. The shaded areas represent the fcc-to-hcp phase transition pressure regime: light (1.5–40 GPa [*Errandonea et al.*, 2002]) and dark (14–75 GPa [*Jephcoat et al.*, 1987]). The seismically derived core-mantle and inner core–outer core boundary pressures are shown for reference [*Dziewonski and Anderson*, 1981].

reaction: $x\mathrm{Fe} + (1 - x)\mathrm{Xe} \iff \mathrm{Fe}_x\mathrm{Xe}_{(1-x)}$ where x is a value between 0.9688 and 0.9958 (32- to 240-atom supercells) (Figure 1). At 0 K we find that at the lowest Xe concentration tested, ~0.4 mol % Xe abundance level in Fe (240-atom supercell), xenon substitution into iron becomes favorable relative to constituent elements above ~300 GPa, a pressure corresponding to the deep outer core (Figure 1). This abundance compares well with the 0.5 mol % Xe concentration obtained by high-voltage experiments of Xe implantation into α-Fe (body-centered cubic phase stable at room conditions) conducted in the late 1960s and 1970s [*Schoeters et al.*, 1976]. If we assume that each side of the equilibrium reaction has similar vibrational entropy, with the only difference being the entropy of mixing stemming from the large number of positions that the Xe can be substituted in the Fe-Xe supercell, the alloy is even more favored (i.e., stability will be achieved at lower pressures) by entropic effects at high temperatures (Figure 2) [*Hume-Rothery*, 1963]; electronic contributions [*Wasserman et al.*, 1996] to entropy are negligible as the electronic density of states of the Fe-Xe supercells are nearly indistinguishable from that of pure Fe at the same volume (see Figure S1 in auxiliary material). Therefore, including temperature and the entropy of mixing, xenon substitution into iron at 350 GPa increases from less than

0.3 (±0.1) mol % Xe at static conditions to more than ~0.6 (±0.2) mol % at 5000 K (Figure 2). The uncertainties in Xe solubility stem from the inherent resolution of the energy convergence (~5 meV/atom) as well as the third-order polynomial fit to the ΔGibbs free energy versus Xe concentration (Figure 2).

[11] Previous experimental and theoretical work on possible Fe-Xe alloys yielded nonalloying behavior between xenon and iron at all pressures relevant to the Earth [*Caldwell et al.*, 1997]. However, the theoretical alloys tested are of extremely high Xe concentration: FeXe, $\mathrm{Fe}_2\mathrm{Xe}$, and FeXe_2 (i.e., ~33–66 mol %). Our calculations yield otherwise for much lower Xe concentration alloys: $\mathrm{Fe}_{0.9958}\mathrm{Xe}_{0.0042}$, $\mathrm{Fe}_{0.9944}\mathrm{Xe}_{0.0056}$, $\mathrm{Fe}_{0.9931}\mathrm{Xe}_{0.0069}$, and $\mathrm{Fe}_{0.9896}\mathrm{Xe}_{0.0104}$ (Figure 1). For the pressures attained in the Earth's core (~364 GPa) we estimate the solubility limit of Xe into Fe at ~0.8 (±0.2) mol % for representative core temperatures. For a smaller planet like Mars the solubility limit is considerably less (<0.1 mol %) because of decreased maximum internal pressures and temperatures.

[12] Our supercell results also show that with increasing Xe concentration the volume of the host Fe unit cell increases and the alloys become more compressible (Figure 3, Table 1). *Caldwell et al.* [1997] did not report any Fe unit cell deviations at ~50 GPa after heating with Xe
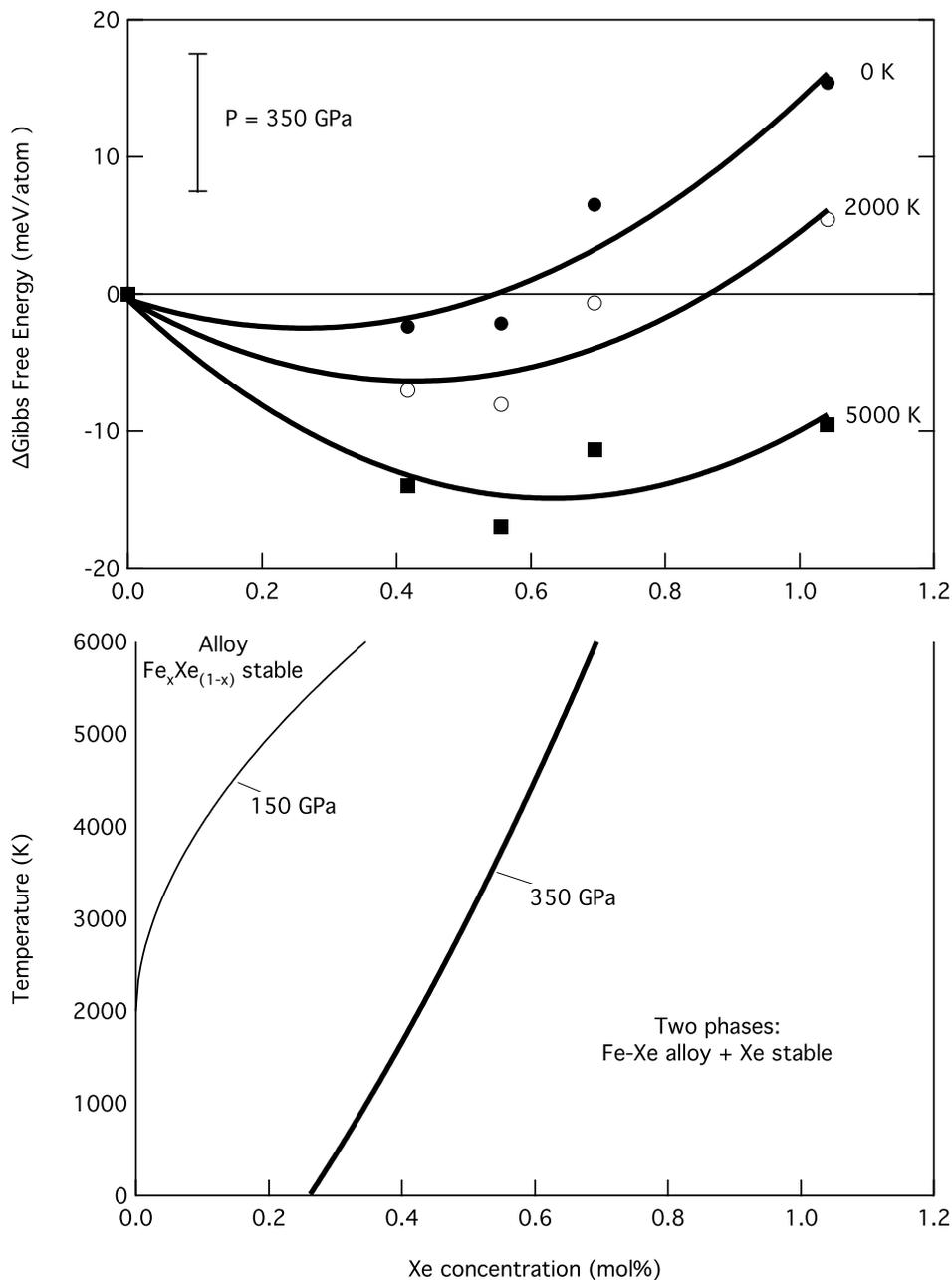
Figure 2. (top) Difference in the Gibbs free energy of the pure elements Fe and Xe compared to the Fe-Xe alloy versus Xe concentration (mol %) at 350 GPa: xFe $+ (1 − x)$Xe $\Longleftrightarrow$ Fe$_x$Xe$_{(1−x)}$, where x is a value between 0.9896 and 1.000 at 0 K (solid circles), 2000 K (open circles), and 5000 K (squares). Labeled curves through the data are third-order polynomial fits. The minima of each polynomial fit are used to construct the phase diagram below. A representative error bar is shown for energy convergence uncertainty ($\pm\sim$5 meV). (bottom) Fe-Xe alloy phase diagram of temperature versus Xe concentration. Thick curve delineates the stability boundary between the Fe-Xe alloy and a two-phase space at 350 GPa. For comparison we also include the boundary at 150 GPa (thin curve). To the left of each curve the Fe-Xe alloy is stable, whereas to the right of each curve a mixed region of Fe-Xe alloy and Xe phases are stable. The curvature of the phase boundaries is determined by the quality of the polynomial fit from above.

above 3000 K. However, for the maximum amount of Xe soluble under these conditions (<0.05 mol %) the expected volume increase (< ~0.1%) may have been too small to detect with the experimental resolution of the time.

[13] As in the previous study [*Caldwell et al.*, 1997], we observe a lack of significant bonding between Xe and the Fe unit cell (Figure 4). Although the nearest-neighbor distance between Xe and the surrounding Fe atoms decreases with increasing pressure as expected, the slope of the line is
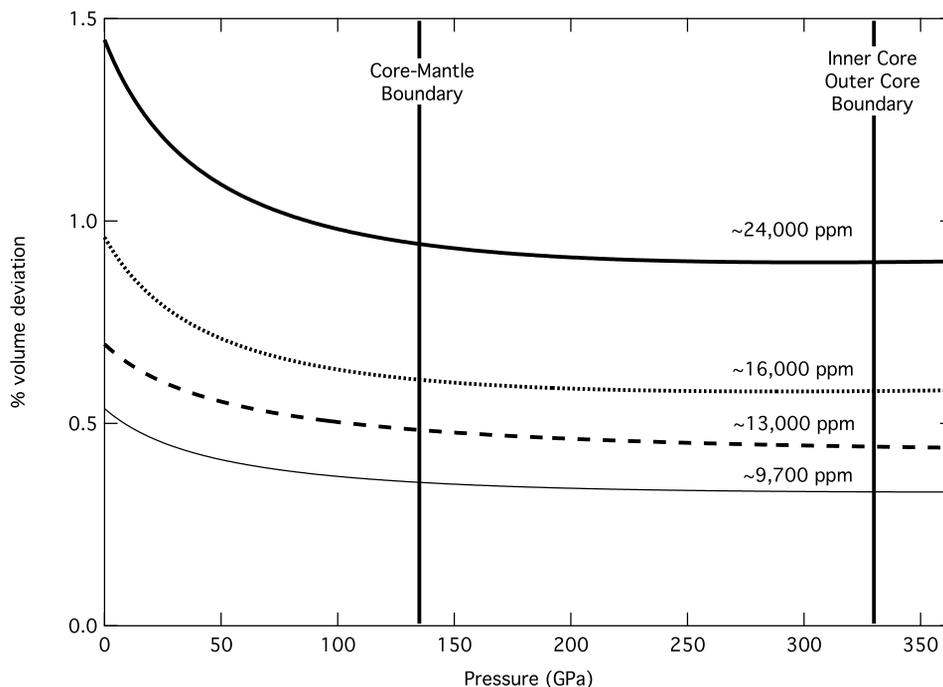
Figure 3. Percent volume difference, $100[V(Fe_x Xe_{(1-x)}) - V(Fe)]/V(Fe)$, versus pressure for the 96-, 144-, 180-, and 240-atom supercells. Curves are labeled according to Xe concentrations: see Figure 1. The seismically derived core-mantle and inner core–outer core boundary pressures are shown for reference [*Dziewonski and Anderson*, 1981].
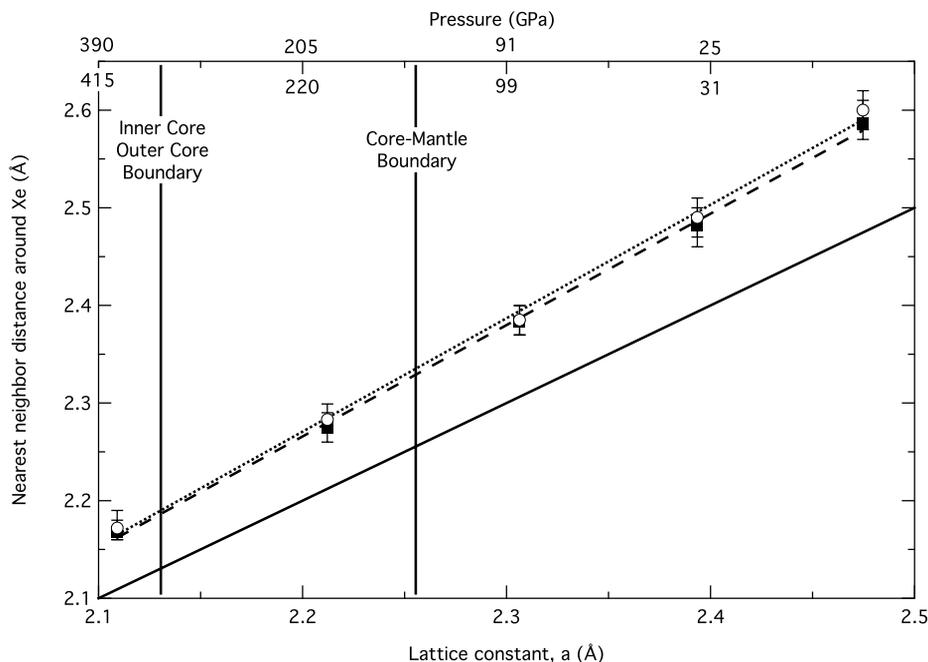

Figure 4. Nearest-neighbor distance around Xe versus lattice constant for the 48-atom (squares) and 180-atom (circles) supercells: $Fe_{0.9792}Xe_{0.0208}$ and $Fe_{0.9944}Xe_{0.0056}$. Error bars give the spread around the average nearest-neighbor value. The dotted (dashed) lines yield a best fit line to the 180-atom (48-atom) supercells; the solid line is the 1:1 relation between nearest-neighbor distance and lattice constant. Corresponding pressures are given for the Fe-Xe supercells along the top (180-atom) and bottom (48-atom) of the top axis. With increasing pressure the nearest-neighbor distance gets smaller and more like the lattice constant. The seismically derived core-mantle and inner core–outer core boundary pressures are shown for reference [*Dziewonski and Anderson*, 1981].

nearly parallel with the 1:1 ratio, indicating that if true bonding between the two elements occurs, it will only do so at higher pressures than those investigated by this study. This is also supported by the lack of Xe contributions to the electronic density of states near the Fermi energy (Figure S1 in auxiliary material).

4. Discussion

[14] The Earth's atmosphere is missing a significant portion (>90%) of its Xe budget. If the atmosphere is assumed to approximate the total terrestrial noble gas inventory, then it follows that this >90% depletion characterizes the bulk Earth as well. Calculations based on this bulk Xe abundance and the decay systematics of short-lived nuclides ^{129}I and ^{244}Pu then suggest a formation interval for the Earth more in line with estimates from other radiogenic systems [Kleine et al., 2002; Ozima and Podosek, 1999; Yin et al., 2002]. However, instead of a preferential loss to space of Xe over lighter noble gases we propose that much of the Xe may be trapped in the core; thus the Earth may not be fully degassed, and the atmospheric abundance may be a poor approximation of the Earth's Xe budget. If parent elements I, Pu, and U were also sequestered into the core [McDonough, 2004] during core formation, the Xe daughter products may also remain in the core on the basis of the high solubility limit we have established here. Therefore, instead of the standard model of Xe being lost during accretion we have the possibilities that either the xenon could have sunk into a differentiating core by forming a solid solution with iron during the sufficiently violent and energetic accretion process or it is present in the core as a radioactive decay product. It is worth noting that the tested Xe concentrations are much greater than what is expected for the Earth. As such, computational trends suggest that lower concentrations require lower pressures to alloy; therefore Xe solubility in Fe may occur at much lower pressures in the Earth.

[15] There are limited partitioning results between silicates and metal for noble gases at high pressures (<10 GPa) and temperatures (1900 K) [Matsuda et al., 1993]. Matsuda et al. [1993] find that the partition coefficients (metal-silicate) decrease with increasing pressure, although their uncertainties rise with pressure. This decrease in partitioning is attributed to higher surface tension from the increased pressure. For higher-pressure experiments we expect the surface tension to change since Fe transforms to the close-packed hcp phase at ~13 GPa [Bancroft et al., 1956] and is also inferred to undergo a spin transition from magnetic to nonmagnetic at this structural transition [Taylor et al., 1991]. Along these lines, another study investigated the argon solubility in silicate melt and found that above ~5 GPa an abrupt change in the argon solubility occurred [Chamorro-Perez et al., 1996]. Argon was no longer as incompatible in the crystalline silicate compared to the melt as had been observed at low pressures [Carroll and Stolper, 1993], and this effect is predicted to occur at lower pressures for the larger Xe atom. There is also additional experimental evidence that Xe can be incorporated into silicates at percent levels at high pressures [Sanloup et al., 2002]. These experimental studies and our results suggest several exceptions to the standard differentiation history for

Xe, and hence there is a significant possibility that the Earth's "missing" xenon may be hidden in the Earth's deep interior rather than lost to space during accretion.

[16] Our results can readily explain the "missing" Xe problem in the Earth, as cosmochemical constraints only allow ~10^{-1} ppm (equivalently 100 ppb, by weight) in the Earth's core compared to the solubility limit of ~10^4 ppm (by weight) that the ε-Fe unit cell volume will accommodate at core conditions (Figures 1 and 2). Although our results can resolve the "missing" Xe problem by placing Xe in the core, we do not constrain the isotopic core abundances of the Xe daughter isotopes, namely, ^{129}Xe (from ^{129}I) and ^{131,132,134,136}Xe (from ^{244}Pu and ^{238}U). However, because of the vastly different electronic structures of iodine, plutonium, and uranium we can imagine a preferred partitioning into the Earth's core of one parent over another. A recent model [Trieloff and Kunz, 2005] also suggests that some (of all) of the noble gases may have been sequestered into a young accreting core when the noble gas abundance was great (before the Moon-forming impact) and that the core is currently "degassing" into the mantle because of unfavorable metal-silicate partitioning coefficients [Matsuda et al., 1993] evident by a higher (and at a constant factor of ~5 across all noble gases) primordial noble gas isotope versus radiogenic isotope ratio in plume basalts when compared to mid-ocean ridge basalts (e.g., ^{3}He/^{4}He and ^{130}Xe/^{136}Xe). Our results contradict this model for Xe: No degassing of any Xe isotope from the core should take place. Indeed, more precise measurements and theoretical calculations on the partitioning of Xe, I, Pu, and U between metal and silicates at high pressures and temperatures are necessary for a better understanding of the Earth's bulk and isotopic xenon budget.

References

Alfe, D., M. J. Gillan, and G. D. Price (2000a), Constraints on the composition of the Earth's core from ab initio calculations, Nature, 405, 172–175.

Alfe, D., G. Kresse, and M. J. Gillan (2000b), Structure and dynamics of liquid iron under Earth's core conditions, Phys. Rev. B, 61(1), 132–142.

Balog, P. S., R. A. Secco, D. C. Rubie, and D. J. Frost (2003), Equation of state of liquid Fe-10 wt % S: Implications for the metallic cores of planetary bodies, J. Geophys. Res., 108(B2), 2124, doi:10.1029/2001JB001646.

Bancroft, D., E. L. Peterson, and S. Minshall (1956), Polymorphism of iron at high pressure, J. Appl. Phys., 27, 291–298.

Bernatowicz, T. J., F. A. Podosek, M. Honda, and F. E. Kramer (1984), The atmospheric inventory of xenon and noble gases in shales: The plastic bag experiment, J. Geophys. Res., 89, 4597–4611.

Bernatowicz, T. J., B. M. Kennedy, and F. A. Podosek (1985), Xe in glacial ice and the atmospheric inventory of noble gases, Geochim. Cosmochim. Acta, 49, 2561–2564.

Birch, F. (1952), Elasticity and constitution of the Earth's interior, J. Geophys. Res., 57, 227–286.

Caldwell, W. A., J. H. Ngyuen, B. G. Pfrommer, F. Mauri, S. G. Louie, and R. Jeanloz (1997), Structure, bonding, and geochemistry of xenon at high pressures, Science, 277, 930–933.

Carroll, M. R., and E. M. Stolper (1993), Noble gas solubilities in silicate melts and glasses: New experimental results for argon and the relationship between solubility and ionic porosity, Geochim. Cosmochim. Acta, 57, 5039–5051.

Chamorro-Perez, E., P. Gillet, and A. Jambon (1996), Argon solubility in silicate melts at very high pressures: Experimental set-up and preliminary

results for silica and anorthite melts, *Earth Planet. Sci. Lett.*, *145*, 97–107.

Cohen, R. E., L. Stixrude, and E. Wasserman (1997), Tight-binding computations of elastic anisotropy of Fe, Xe, and Si under compression, *Phys. Rev. B*, *56*(14), 8575–8589.

Cohen, R. E., O. Gulseren, and R. J. Hemley (2000), Accuracy of equation-of-state formulations, *Am. Mineral.*, *85*, 338–344.

Dauphas, N. (2003), The dual origin of the terrestrial atmosphere, *Icarus*, *165*, 326–339.

Dewhurst, J. K., R. Ahuja, S. Li, and B. Johansson (2002), Lattice dynamics of solid xenon under pressure, *Phys. Rev. Lett.*, *88*(7), doi:10.1103/PhysRevLett.88.075504.

Dziewonski, A. M., and D. L. Anderson (1981), Preliminary reference Earth model, *Phys. Earth Planet. Inter.*, *25*(4), 297–356.

Eremets, M. I., E. A. Gregoryanz, V. V. Struzkhin, H.-K. Mao, and R. J. Hemley (2000), Electrical conductivity of xenon at megabar pressures, *Phys. Rev. Lett.*, *85*(13), 2797–2800.

Errandonea, D., B. Schwager, R. Boehler, and M. Ross (2002), Phase behavior of krypton and xenon to 50 GPa, *Phys. Rev. B*, *65*(21), doi:10.1103/PhysRevB.65.214110.

Farley, K. A., and E. Neroda (1998), Noble gases in the Earth's mantle, *Annu. Rev. Earth Planet. Sci.*, *26*, 189–218.

Goettel, K. A., J. H. Eggert, and I. F. Silvera (1989), Optical evidence for the metallization of xenon at 132(5) GPa, *Phys. Rev. Lett.*, *62*(6), 665–668.

Hume-Rothery, W. (1963), *Electrons, Atoms, Metals and Alloys*, 387 pp., Dover, Mineola, N. Y.

Jephcoat, A. P. (1998), Rare-gas solids in the Earth's deep interior, *Nature*, *393*, 355–358.

Jephcoat, A. P., H.-K. Mao, L. W. Finger, D. E. Cox, R. J. Hemley, and C.-S. Zha (1987), Pressure-induced structural phase transitions in solid xenon, *Phys. Rev. Lett.*, *59*(23), 2670–2673.

Kleine, T., C. Munker, K. Mezger, and H. Palme (2002), Rapid accretion and early core formation on asteroids and the terrestrial planets from Hf-W chronometry, *Nature*, *418*, 952–955.

Kresse, G., and J. Furthmuller (1996), Efficient iterative schemes for ab initio total-energy calculations using a plane-wave basis set, *Phys. Rev. B*, *54*(16), 11,169–11,186.

Kresse, G., and J. Hafner (1993), Ab initio molecular dynamics for liquid metals, *Phys. Rev. B*, *47*(1), 558–561.

Kresse, G., and D. Joubert (1999), From ultrasoft pseudopotentials to the projector augmented-wave method, *Phys. Rev. B*, *59*(3), 1758–1775.

Krummenacher, D., C. M. Merrihue, R. O. Pepin, and J. H. Reynolds (1962), Meteoritic krypton and barium versus the general isotopic anomalies in xenon, *Geochim. Cosmochim. Acta*, *26*, 231–249.

Lee, K. K. M., and R. Jeanloz (2003), High-pressure alloying of potassium and iron: Radioactivity in the Earth's core?, *Geophys. Res. Lett.*, *30*(23), 2212, doi:10.1029/2003GL018515.

Lee, K. K. M., G. Steinle-Neumann, and R. Jeanloz (2004), Ab-initio high-pressure alloying of iron and potassium: Implications for the Earth's core, *Geophys. Res. Lett.*, *31*, L11603, doi:10.1029/2004GL019839.

Lin, J.-F., D. L. Heinz, A. J. Campbell, J. M. Devine, and G. Shen (2002), Iron-silicon alloy in Earth's core, *Science*, *295*, 313–315.

Mao, H.-K., Y. Wu, L. C. Chen, J. F. Shu, and A. P. Jephcoat (1990), Static compression of iron to 300 GPa and $Fe_{0.8}Ni_{0.2}$ alloy to 260 GPa: Implications for composition of the core, *J. Geophys. Res.*, *95*, 21,737–21,742.

Matsuda, J., and K. Matsubara (1989), Noble gases in silica and their implication for the terrestrial "missing" Xe, *Geophys. Res. Lett.*, *16*, 81–84.

Matsuda, J., M. Sudo, M. Ozima, K. Ito, O. Ohtaka, and E. Ito (1993), Noble gas partitioning between metal and silicate under high pressures, *Science*, *259*, 788–790.

McDonough, W. F. (2004), Compositional model for the Earth's core, in *Treatise on Geochemistry*, vol. 2, *Geochemistry of the Mantle and Core*, edited by R. W. Carlson, pp. 547–568, Elsevier, New York.

Ozima, M., and F. A. Podosek (1999), Formation age of Earth from $^{129}I/^{127}I$ and $^{244}Pu/^{238}U$ systematics and the missing Xe, *J. Geophys. Res.*, *104*, 25,493–25,499.

Pepin, R. O. (1991), On the origin and early evolution of terrestrial planet atmospheres and meteoritic volatiles, *Icarus*, *92*, 1–79.

Pepin, R. O., and D. Porcelli (2002), Origin of noble gases in the terrestrial planets, in *Noble Gases in Geochemistry and Cosmochemistry, Rev. Mineral. Geochem.*, vol. 47, edited by D. Porcelli, C. J. Ballentine, and R. Wieler, pp. 191–246, Mineral Soc. Am., Washington D. C.

Perdew, J. P., J. A. Chevary, S. H. Vosko, K. A. Jackson, M. R. Pederson, D. J. Singh, and C. Fiolhais (1992), Atoms, molecules, solids, and surfaces: Applications of the generalized gradient approximation for exchange and correlation, *Phys. Rev. B*, *46*(11), 6671–6687.

Porcelli, D., and C. J. Ballentine (2002), Models for the distribution of terrestrial noble gases and evolution of the atmosphere, in *Noble Gases in Geochemistry and Cosmochemistry, Rev. Mineral. Geochem.*, vol. 47, edited by D. Porcelli, C. J. Ballentine, and R. Wieler, pp. 411–480, Mineral Soc. Am., Washington D. C.

Reichlin, R., K. E. Brister, A. K. McMahan, M. Ross, S. Martin, Y. K. Vohra, and A. L. Ruoff (1989), Evidence for the insulator-metal transition in xenon from optical, x-ray, and band-structure studies to 170 GPa, *Phys. Rev. Lett.*, *62*(6), 669–672.

Ross, M., and A. K. McMahan (1980), Condensed xenon at high pressure, *Phys. Rev. B*, *21*(4), 1658–1664.

Sanloup, C., R. J. Hemley, and H. Mao (2002), Evidence for xenon silicates at high pressure and temperature, *Geophys. Res. Lett.*, *29*(18), 1883, doi:10.1029/2002GL014973.

Schoeters, E., R. Coussement, R. Geerts, J. Odeurs, H. Pattyn, R. E. Silverans, and L. Vanneste (1976), Hyperfine interactions of xenon in iron, *Phys. Rev. B*, *37*(5), 302–305.

Steinle-Neumann, G., L. Stixrude, and R. E. Cohen (1999), First-principles elastic constants for the hcp transition metals Fe, Co, and Re at high pressure, *Phys. Rev. B*, *60*(2), 791–799.

Taylor, R. D., M. P. Patsernak, and R. Jeanloz (1991), Hysteresis in the high pressure transformation of bcc- to hcp-iron, *J. Appl. Phys.*, *69*(8), 6126–6128.

Tolstikhin, I. N., and R. K. O'Nions (1994), The Earth's missing xenon: A combination of early degassing and of rare gas loss from the atmosphere, *Chem. Geol.*, *115*, 1–6.

Trieloff, M., and J. Kunz (2005), Isotope systematics of noble gases in the Earth's mantle: Possible sources of primordial isotopes and implications for mantle structure, *Phys. Earth Planet. Inter.*, *148*, 13–38.

Tsuchiya, T., and K. Kawamura (2002), First-principles study of systematics of high-pressure elasticity in rare gas solids, Ne, Ar, Kr, and Xe, *J. Chem. Phys.*, *117*(12), 5859–5865.

Vinet, P., J. H. Rose, J. Ferrantes, and J. R. Smith (1989), Universal features of the equation of state of solids, *J. Phys. Condens. Matter*, *1*, 1941–1963.

Wacker, J. F., and E. Anders (1984), Trapping of xenon in ice: Implications for the origin of the Earth's noble gases, *Geochim. Cosmochim. Acta*, *48*, 2373–2380.

Wasserman, E., L. Stixrude, and R. E. Cohen (1996), Thermal properties of iron at high pressures and temperatures, *Phys. Rev. B*, *53*(13), 8296–8309.

Yin, Q., S. B. Jacobsen, K. Yamashita, J. Blichert-Toft, P. Telouk, and F. Albarede (2002), A short timescale for terrestrial planet formation from Hf-W chronometry of meteorites, *Nature*, *418*, 949–952.

_____

K. K. M. Lee, Physics Department, New Mexico State University, MSC 3D, Box 30001, Las Cruces, NM 88003-0001, USA. (kanani@physics.nmsu.edu)

G. Steinle-Neumann, Bayerisches Geoinstitut, Universität Bayreuth, Bayreuth D-95440, Germany.